Porous Silaphosphorene, Silaarsenene and Silaantimonene: a Sweet Marriage of Si and P/As/Sb

Shiru Lin,[†] Jinxing Gu,[†] Yu Wang,[†] Yanchao Wang,[‡] Shengli Zhang,[§] Xinghui Liu,[ǁ,⊥]

Haibo Zeng,[§] Zhongfang Chen[†,*]

[†] Department of Chemistry, University of Puerto Rico, Rio Piedras, San Juan, PR 00931, USA
[‡] State Key Lab of Superhard Materials, Jilin University, Changchun 130012, China
[§] Institute of Optoelectronics & Nanomaterials, Jiangsu Key Laboratory of Advanced Micro & Nano Materials and Technology, College of Material Science and Engineering, Nanjing University of Science and Technology, Nanjing 210094, China
[ǁ] Centre for Integrated Nanostructure Physics (CINAP), Institute of Basic Science (IBS), 2066 Seoburo, Jangan-Gu, Suwon 16419, Republic of Korea.
[⊥] Department of Chemistry, Sungkyunkwan University (SKKU), 2066 Seoburo, Jangan-Gu, Suwon 16419, Republic of Korea

* To whom correspondence should be addressed. Email: zhongfangchen@gmail.com (Z.C.)

Abstract

Inspired by the recent experimental realization of pnictogen-silicon analogues of benzene and great interests in silicene, phosphorene and its heavier counterparts, herein we designed three planar porous 2D nanomaterials, namely porous silaphosphorene (pSiP), silaarsenene (pSiAs) and silaantimonene (pSiSb), and systematically investigated their stability, electronic, and optical properties, as well as their potential as photocatalysts for water-splitting. Porous silaphosphorene, silaarsenene and silaantimonene monolayers are all thermodynamically, dynamically and thermally stable, and the aromaticity in each six-membered Si_3P_3/Si_3As_3/Si_3Sb_3 ring plays an important role to their enhanced stability. They are all semiconductors with direct band gaps of 1.93, 1.57 and 0.95 eV (HSE06) and have comparable carrier mobility to MoS_2. Their good stability and exceptional electronic, optical and mechanical properties endow them promising candidates for applications in solar cells and other optoelectronics fields. Moreover, the suitable band edge alignments of pSiP and pSiAs monolayers endow them potential applications as photocatalysts for water-splitting.

TOC

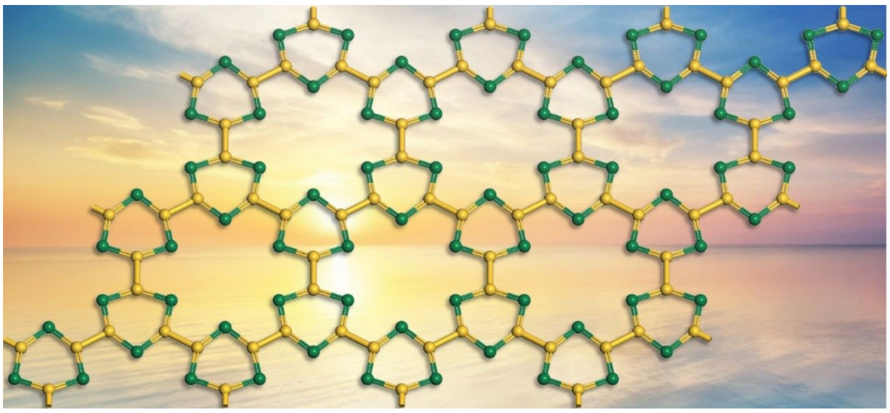

1. Introduction

With unique material characteristics, two-dimensional materials (2D) have emerged with far-reaching potentials, and are among the most exciting and promising areas of research. Since the experimental realization of graphene in 2004,[1] the family of 2D materials has greatly expanded,[2-11] many layered structures such as hexagonal boron nitride, transition metal dichalcogenides and phosphorene, have been fabricated, and more 2D materials have been predicted, though not yet synthesized.[12-15]

As semiconductor industry is currently based on silicon (Si), it is not a surprise that the Si counterpart of graphene, namely silicene,[16,17] has attracted increasing interests in last years. Silicene shares most of the outstanding electronic properties of graphene, *eg*. it is also semi-metallic with a Dirac point.[18,19] However, different from the planar graphene, silicene has a low buckled honeycomb geometry,[20,21] since silicon prefers to adopt sp^3 hybridization rather than sp^2 hybridization.[20,22,23] So far, the free-standing silicene has not been achieved, only the substrate supported silicene has been synthesized.[24-31]

Another interesting 2D material that would compete with graphene is black phosphorene (BP)[8,9,32-33] BP adopts a puckered structure along the armchair direction and displays a bilayer-shape along the zigzag direction, thus possessing significant anisotropic properties.[33-37] The bandgap of phosphorene monolayer is 1.45 eV as measured by photoluminescence spectra,[32] while the bandgap decreases with increasing the number of layers.[38-40] Its suitable bandgap and high carrier mobility[33] endow phosphorene many promising applications, especially in electronics and optoelectronics. Recently, the monolayers of heavier group 15 elements (arsenene, antimonene, and bismuthene)[41] have been theoretically predicted,[42-43] among which the antimonene has been experimentally fabricated by mechanical exfoliation, liquid exfoliation, plasma-assisted process,[44] and vapor deposition techniques.[45-47] These monolayers cover a broad range of band gaps and are of superior carrier mobility, thus are promising candidates for nanoelectronics and optoelectronics.

On the other side, hydrogen generated through photocatalytic water-splitting reaction is an important key for solving energy crisis and environmental pollution problems.[48-51] Along this line, strain engineered BP monolayer has been designed as a potential photocatalyst for water-splitting.[52-53]

Very recently, Scheer and coworkers successfully synthesized the pnictogen-silicon analogues of benzene, namely $[(PhC(NtBu)_2)_3Si_3P_3]$ and $[(PhC(NtBu)_2)_3Si_3As_3]$ molecules.[54] The enhanced stabilities and quasi-planar geometry of Si_3P_3/Si_3As_3 unit inspired us to employ them as building blocks to design the planar 2D materials combined silicon and phosphorus/arsenic/antimony atoms.

Herein by means of systematic density functional theory (DFT) computations, we theoretically designed three planar 2D nanomaterials, namely porous silaphosphorene, silaarsenene and silaantimonene (denoted as pSiP, pSiAs and pSiSb hereafter). We verified their stabilities by calculating binding energies, phonon modes and performing *ab initio* molecular dynamics (AIMD) simulations, and investigated their electronic and optical properties, as well as band edge alignments. Our computations revealed that pSiP, pSiAs, pSiSb monolayers are semiconducting with direct bandgaps (1.93, 1.57

and 0.95 eV, respectively) which can be tuned by external strains, have comparable carrier mobility to MoS_2, and have high efficient absorption in visible light region. These exceptional properties endow them many applications such as in nanoelectronics, optoelectronics, solar cells and photocatalysis for water-splitting.

2. Computational methods

Our DFT computations were carried out by Vienna ab initio simulation package (VASP).[55] The projector-augmented plane wave (PAW)[56] was used to model the ion-electron interactions. The electron exchange-correlation functional was treated using generalized gradient approximation (GGA) in the form proposed by Perdew, Burke and Ernzerhof (PBE).[57] The 4×4×1 and 9×9×1 Monkhost-Pack k points were used for geometry optimizations and self-consistent calculations, respectively. The energy cutoffs of the plane wave for pSiP, pSiAs and pSiSb were 500, 600 and 500 eV, respectively. The convergence tolerances were set as 10^{-6} eV for phonon modes calculations and 10^{-5} eV for other calculations. We placed the 2D monolayers in the *xy* plane with the *z* direction perpendicular to the layer plane, and vacuum spaces of over 12 Å in the *z* direction were adopted so that there is no significant interaction between adjacent layers. Both spin-polarized and spin-unpolarized computations were performed, and the computational results showed that pSiP, pSiAs and pSiSb are all nonmagnetic.

To examine the dynamic stability of pSiP, pSiAs and pSiSb, we computed the phonon dispersions at the PBE level of theory by CASTEP code[58] using 4×4×1 Monkhost-Pack k points and 10^{-6} eV convergence tolerances. We also performed *ab* *initio* molecular dynamics (AIMD) simulations to evaluate the thermal stabilities utilizing DMol^3 code.[59-60] In the AIMD simulations, the PBE functional and NVT canonical ensemble were used, and a 2×2×1 supercell was annealed at various temperatures, each simulation lasted 10 *ps* with a time step of 2.0 *fs*.

The particle-swarm optimization (PSO) method as implemented in CALYPSO code[61] was used to search for low-energy 2D planar SiP, SiAs and SiSb monolayer sheets. The optimizations were performed by VASP code using PBE functional. In our calculations, the population size was set to 50, and the number of generation was set to 50. Unit cells containing 6 silicon atoms and 6 phosphorus/arsenic/antimony atoms were considered. The CALYPSO search helped us to check whether the pSiP, pSiAs and pSiSb are global minima among corresponding 2D planar structures.

Since the PBE functional trends to underestimate bandgaps of materials,[62] we recomputed the band structures using the Heyd-Scuseria-Ernzerhof (HSE06)[63] screened-hybrid functional, which was proven to be a reliable method for the calculations of electronic and optical properties. We also explored the optical absorption properties of pSiP, pSiAs and pSiSb by calculating the dielectric functions using HSE hybrid functional with 21×21×1 k-points mesh for pSiP and 13×13×1 k-points mesh for pSiAs and pSiSb.

3. Results and discussion

3.1. Geometric structures and chemical bonding analysis

pSiP, pSiAs and pSiSb monolayers are all purely planar porous structures, and the pore diameters are 7.64, 7.79, 8.09 Å, respectively. The optimized structures of pSiP/pSiAs/pSiSb monolayers possess six-membered rings, or Si_3P_3/Si_3As_3/Si_3Sb_3

subunits, with alternating Si and P/As/Sb atoms (Figure 1). In all these structures, the six-membered rings are linked covalently by Si-Si bonds (2.35, 2.34, 2.50 Å for pSiP, pSiAs and pSiSb respectively), so that each Si atom binds to two P/As/Sb atoms and another adjacent Si atom, and each P/As/Sb atom binds to two Si atoms. In pSiP, the Si-P bond lengths are uniformly 2.16 Å, the P-Si-P and Si-P-Si bond angles are 140.0° and 100.0°, respectively. Note that the bond lengths and bond angles in the Si_3P_3 subunit are very close to the corresponding values in [(PhC(NtBu)$_2$)$_3$Si$_3$P$_3$], the Si-P analogue of benzene (2.15~2.16 Å, 134~135°, 102~103°),[54] and well agree with the recent theoretical study by Wang and coworkers.[64] Similarly, in pSiAs, the Si-As bond length (2.28 Å) as well as the As-Si-As and Si-As-Si bond angles (140.3° and 99.7°) of the Si_3As_3 subunit are also very close to those in the [(PhC(NtBu)$_2$)$_3$Si$_3$As$_3$] molecule (2.16~2.26 Å, 135~139°, 101~102°). In pSiSb, the Si-Sb bond lengths (2.33 Å) and the Sb-Si-Sb and Si-Sb-Si bond angles (139.8° and 100.2°) are also close to those in $H_3Si_3Sb_3$ molecule as we calculated (2.48 Å, 141.4°, 98.6°). Moreover, all Si-P (2.16 Å), Si-As (2.28 Å) and Si-Sb (2.33 Å) bonds are shorter than those of their corresponding silicene-like structures (Figure S1) (2.27,[65] 2.39 and 2.59 Å respectively). These structural similarities indicate that the Si_3P_3, Si_3As_3 and Si_3Sb_3 subunits also share aromatic characters of the pnictogen-silicon analogues of benzene (Table S1).[54]

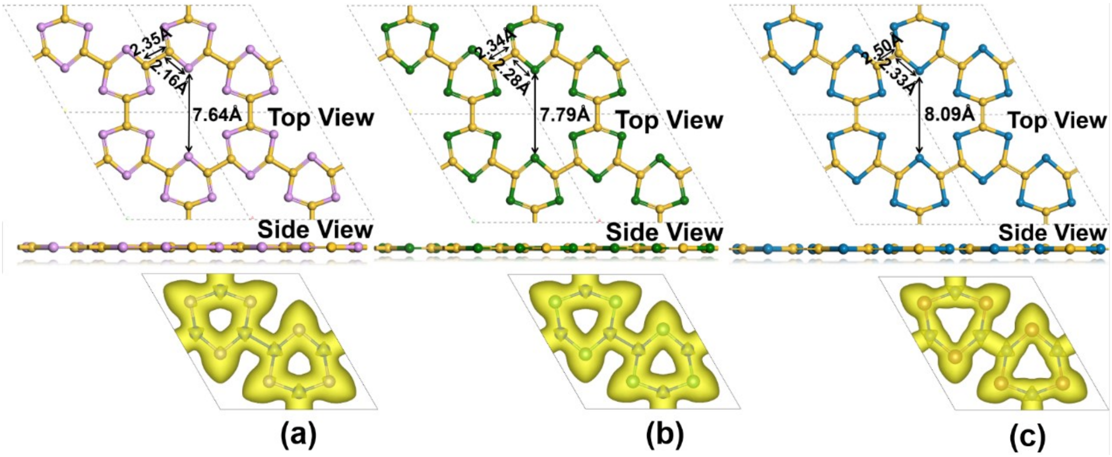

Figure 1. Optimized structures of (a) pSiP, (b) pSiAs, and (c) pSiSb. The pink, green, blue and yellow atoms represent P, As, Sb and Si atoms, respectively. The dashed gray lines limit a 2 × 2 × 1 supercell. Below the side views are the isosurfaces of electron location function (ELF) of unit cell plotted with a value of 0.57 au.

To further understand the chemical bonding, we plotted the deformation electronic density (Figure S2) and total electronic density (Figure 2) of pSiP, pSiAs and pSiSb. The deformation electron density is the difference of total electron density of pSiP/SiAs/SiSb and isolated atoms from the monolayers. As shown in the deformation electronic density plot (Figure S2), some electrons of Si atoms are extracted to P/As/Sb atoms, P/As/Sb atoms have in-plane lone electron pairs towards the pore centers, which indicate that the P/As/Sb atom has hybrid sp^2 orbitals, and the single electron left in their p_z orbital enables the electron delocalization with Si atoms. The electron densities of the six-membered rings are obviously higher than those of Si-Si bonds for all three monolayers (Figure 2), which implies strong electron delocalization of the individual Si_3P_3/Si_3As_3/Si_3Sb_3 rings. The above obtained chemical bonding characteristics are also confirmed by our plots of electron localization functions[66] (Figure 1).

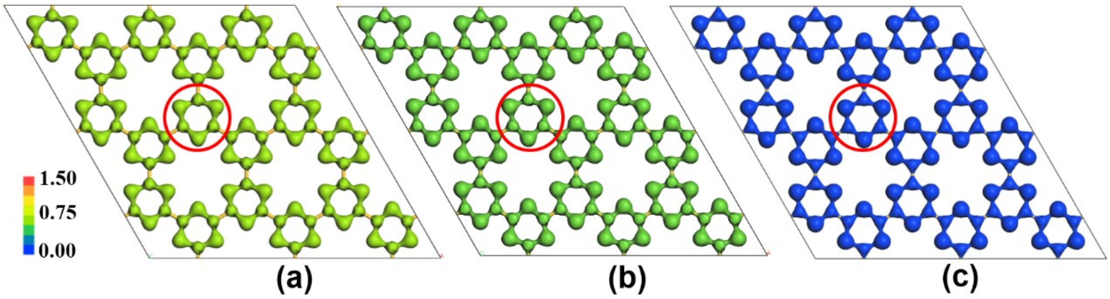

Figure 2. Total electronic density projected on (a) pSiP, (b) pSiAs and (c) pSiSb surface.

3.2. Thermodynamic, dynamic and thermal stabilities

To examine the thermodynamic stability of pSiP, pSiAs and pSiSb, we first calculated their binding energies (E_b) using following equation:

$$E_b = (n_A E_A + n_B E_B - E_{AB}) / (n_A + n_B) \quad (1)$$

where A and B stand for two constituent elements, $E_{A/B}$ and E_{AB} are the total energies of a single atom and material unitcell (One unitcell is composed of 6 silicon atoms and 6 phosphorus/arsenic/antimony atoms). According to this definition, the material with a more positive binding energy is thermodynamically more stable. The computed binding energies of pSiP, pSiAs and pSiSb (3.65, 3.35, 3.03 eV/atom, respectively) are comparable with those of silicene (3.87 eV/atom),[67] phosphorene (3.61 eV/atom),[33,32,68] arsenene (2.99 eV/atom)[69] and antimonene (2.64 eV/atom)[42,70] monolayers at the same theoretical level. Very recently, the silicene-like SiP monolayer with the same binding energy as pSiP (3.65 eV/atom) was predicted,[65] while the silicene-like SiAs and SiSb monolayer (binding energy of 3.32 and 3.02 eV/atom, repectively, see Supporting Information, Figure S1) are slightly less favorable than our predicted pSiAs and pSiSb.

Compared with their single-element counterparts and silicene-like SiP/SiAs, pSiP and pSiAs monolayers have exactly planar structures and fewer interatomic interactions since P, As and Sb atoms are only two-coordinated in the porous structures. It is the aromaticity of the individual six-membered Si_3P_3/Si_3As_3/ Si_3Sb_3 rings that stabilizes the pSiP, pSiAs and pSiSb monolayers.

Table 1. Binding energies of some homoelemetal monolayers, porous monolayers and correspounding silicene-like monolayers.

Binding energy (eV/atom)					
Silicene[67]	3.87	Silicene-like		Porous-	
Phosphorene[33,32,68]	3.61	SiP[65]	3.65	pSiP	3.65
Arsenene[69]	2.99	SiAs	3.32	pSiAs	3.35
Antimonene[42,70]	2.64	SiSb	3.02	pSiSb	3.03

Then, we examined the dynamic stabilities of pSiP, pSiAs and pSiSb monolayers by computing their phonon dispersions. The absence of imaginary modes (Figure S3) conforms that these monolayers are dynamically stable.

We also ascertained their thermal stabilities by performing AIMD simulations for 10 *ps* at 500 K, 800K, 1000 K and 1500 K. Our simulations showed that throughout 10 *ps* AIMD simulations, both pSiP and pSiAs monolayers can maintain their structural integrity up to 1000 K, and pSiSb can maintain its geometry up to 800 K, though the structures are becoming corrugated or distorted with increasing temperature (Figure 3).

However, at 1500 K, the hexagonal frameworks of pSiP and pSiAs are destroyed, and at 1000 K, the framework of pSiSb is devastated. These simulations indicate that pSiP, pSiAs and pSiSb monolayers all have high thermal stabilities, and will not have enough energy to overcome the barrier and become seriously disordered until the temperature is higher than 1000 K (800 K for pSiSb) in a 10 *ps* time frame, thus they may be utilized under high temperatures. Note that our computational results on the phonon dispersions and thermal stabilities of the pSiP monolayer are consistent with those by Wang and coworkers (but the AIMD simulations were performed at 300 K for 5 *ps*).[64]

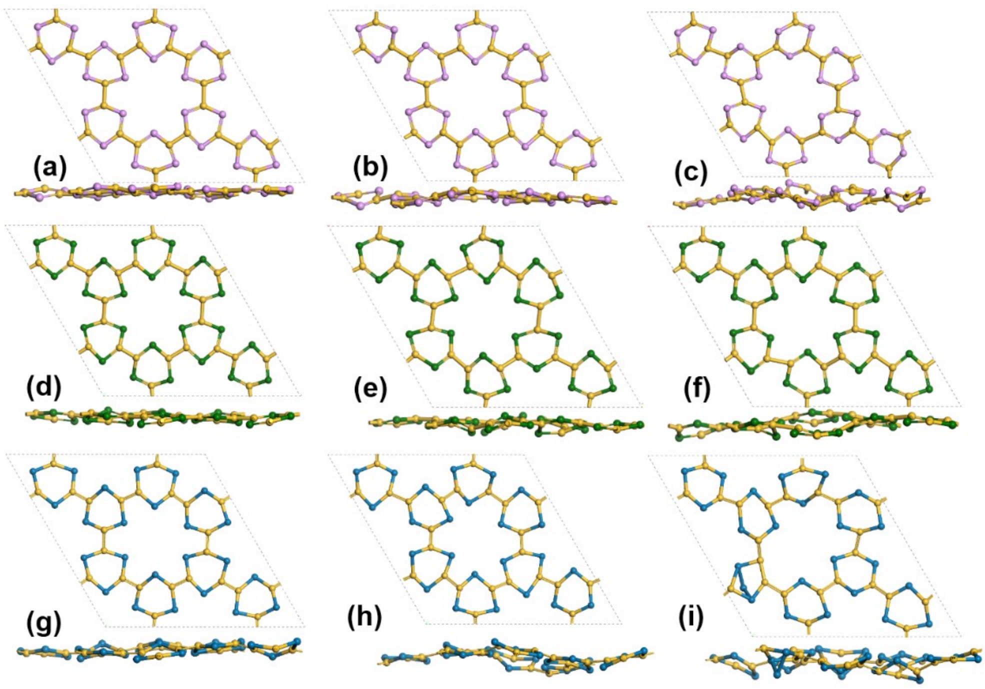

Figure 3. Snapshots of (a-c) pSiP and (d-f) pSiAs (g-i) pSiSb equilibrium structures at (a, d, g) 500 K, (b, e, h) 800 K and (c, f, i) 1000 K at the end of 10 *ps* AIMD simulations.

Recently, other 2D materials with the stoichiometry of SiP were theoretically predicted, including the monolayer exfoliated from the bulk (E_b= 4.21 eV/atom),[71] and the buckled 2D materials predicted by CALYPSO code among which the lowest energy configuration has two silicene-like SiP monolayers connected by covalent Si-Si bonds (E_b= 4.19 eV/atom).[72] Though those structures have larger binding energies, they are not planar single layer structures as studied in this work. Encouragingly, our PSO search revealed that the pSiP, pSiAs and pSiSb monolayers as we constructed are the global minima among corresponding 2D planar structures.

Their good thermodynamic, dynamical and thermal stabilities, combined with the global minimum nature in the 2D space, strongly indicate the high feasibility to experimentally realize pSiP, pSiAs and pSiSb.

3.3. Electronic and optical properties

To explore the electronic properties of pSiP, pSiAs and pSiSb, we computed their band structures and the corresponding total and partial density of states (DOS and PDOS) at HSE06 level of theory (Figure 4). Quite different from silicene which is semi-metallic with a Dirac point, pSiP, pSiAs and pSiSb monolayers are all direct semiconductors, and their band gaps are 1.93, 1.57 and 0.95 eV, respectively, at HSE06 level of theory (1.41, 1.13 and 0.65 eV, respectively, at PBE level of theory). Captivatingly, the band gap of pSiP (1.93 eV) is larger than that of phosphorene (1.45 eV),[32] but pSiAs (1.57 eV) is dramatically smaller than that of arsenene (2.49 eV indirect band),[42] and the band gap of pSiSb (0.95 eV) is also much smaller than antimonene (2.28 eV indirect band at the same theoretical level).[42] Different from the metallic silicene-like SiP monolayer[65] and the semiconducting SiP monolayer exfoliated from the bulk (with a direct band gap of 2.59 eV),[71] our predicted pSiP has a more suitable band gap for solar cell applications, which is consistent with previous work done by Wang's group.[64] A careful analysis of the DOSs of pSiP/As/Sb monolayers (Figure 4) reveals that the states close to the Fermi level are mainly attributed to the hybrid *p* orbitals of silicon and phosphorus/arsenic/antimony atoms. Note that the band gap values of pSiP, pSiAs and pSiSb decrease gradually (Figure 4), which can be understood by the fact that heavier atoms (Sb > As > P) contribute to the weakening of covalent characteristics, leading to smaller band gaps (pSiP > pSiAs > pSiSb). This trend was found in the group 15 monolayers.[42]

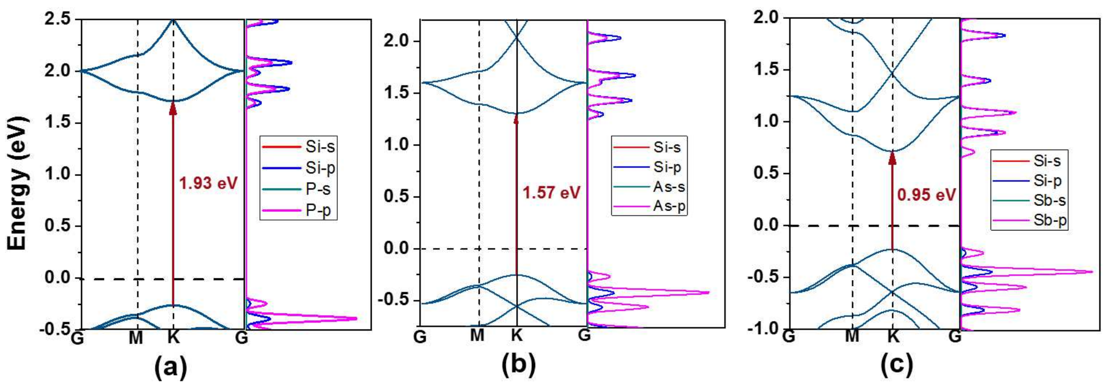

Figure 4. Band structures and partial density of states of (a) pSiP, (b) pSiAs and (c) pSiSb (HSE functional).

Note that we employed both PBE and HSE06 functionals to evaluate the band gaps of pSiP/SiAs/SiSb monolayers. These two functionals led to the same band gap trend and similar shapes for the CBM (conduction band minimum) and VBM (valence band minimum) curves, the major difference is the band gap values (see Supporting

Information, Figure S6). Considering that PBE can correctly predict the band gap variation tendency, and well reproduce the experimentally measured carrier mobilites of various 2D materials, such as graphene,[73,74] phosphorene[33,34] and MoS_2,[75,76] this functional will be employed to investigate the strain effect to the band structures and the carrier mobilities of our newly predicted monolayers.

We also examined the spin-orbit coupling (SOC) effect for pSiSb at the PBE level of theory (Figure S7). Though the inclusion of SOC splits the degenerated bands located in K point, G-M and K-G paths, the change of shapes and positions of CBM and VBM are insignificant, the band gap including SOC effect (0.64 eV) is nearly the same as that without SOC effect (0.65 eV). Thus, SOC effect is negligible for calculating the band gap value and carrier mobility of pSiSb monolayer.

Since applying strain is an effective way for band structure engineering, we examined the relationship between the bandgaps and the applied in-plane biaxial strains along the two vectors of the unitcell. The computations of strain effect were performed under a constant unit cell with volume constraint, and the axial unit cell length l is determined by the percentage strain η ($l = l_0 (1 + \eta)$), where l_0 is the unit cell length of the optimized, unstrained nanostructure. Figure 5 presents the PBE bandgaps of pSiP, pSiAs and pSiSb monolayers under different strains in the range of -2% to 4%. All these three monolayers retain their direct band gap nature under such external strains, stretching increases bandgaps, while compressing results in smaller bandgaps. Under the compression of 2% (-2% strain), these monolayers have the minimum gaps (1.37, 1.08, 0.54 eV, respectively, for pSiP, pSiAs and pSiSb). By 4% stretching (4% strain), the bandgaps achieve the maxima (1.48, 1.20 and 0.90 eV, respectively). The bandgaps of pSiP are about 0.30 eV larger than that of pSiAs, while pSiAs are about 0.54~0.31 eV larger than pSiSb. The differences between the minimum and the maximum band gaps under the -2 to 4% biaxial strain are only about 0.11 eV for pSiP and pSiAs, while 0.36 eV for pSiSb, which suggest that pSiP and pSiAs monolayers have more robust bandgaps than pSiSb against external biaxial strains.

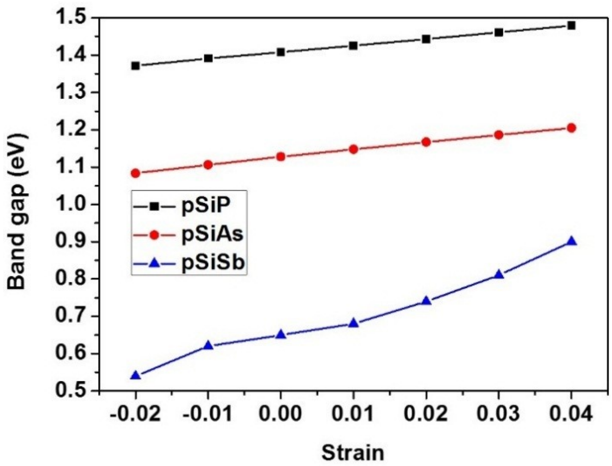

Figure 5. The relationship between the bandgaps (PBE) and the biaxial strains for pSiP (red line), pSiAs (black line) and pSiSb (blue line).

Carrier mobility is an important parameter for semiconductors and photocatalysts. Typically, higher mobility enhances device and photocatalysis performances. To explore the potentials of pSiP, pSiAs and pSiSb monolayers for future applications in optoelectronics, we computed their carrier mobility (electrons and holes) on the basis of deformation potential (DP) theory proposed by Bardeen and Shockley,[77] which has been widely used to calculate the carrier mobility of various 2D materials.[75,78-80]

According to our computations, the effective masses (m^*) of electrons and holes for pSiP/pSiAs/pSiSb monolayer along x direction are 0.61/0.54/0.51 and 0.80/0.86/0.76 m_0 (m_0 is the free electron mass), while those along y direction are 0.45/0.63/0.56 m_0 and 1.35/1.26/0.65 m_0, respectively. We further studied the elastic constants (C) and the deformation potentials (E_1). The deformation potentials (E_1) of pSiP, pSiAs and pSiSb are small, and those of electrons are roughly 45%~65% of holes. Based on the above obtained m^*, C and E_1 values, we estimated the carrier mobility as listed in Table 2. The electron mobilities for pSiP/pSiAs/pSiSb along x and y directions are 271.80/493.96/494.78 and 496.40/401.4/419.41 $cm^2V^{-1}s^{-1}$, while the hole mobilities along x and y directions are 66.74/62.64/47.34 and 22.86/31.26/67.13 $cm^2V^{-1}s^{-1}$, respectively. The same as MoS_2 monolayer, the mobilities of electrons and holes for pSiP, pSiAs and pSiSb are anisotropic. Different from MoS_2 whose hole mobilities are larger than electron mobilities, the mobilities of holes for pSiP/pSiAs/pSiSb are smaller than those of electrons because of the larger deformation potential (E_1). Compared with the MoS_2 monolayer, the mobilities of holes for pSiP/pSiAs/pSiSb are smaller, while the mobilities of electrons for pSiP/pSiAs/pSiSb are more than four times larger.[75] The relatively high mobilities of pSiP, pSiAs and pSiSb enhance the possibilities of using them in electronics, optoelectronics and photocatalysis.

Table 2. The effective mass (m^*), elastic constant(C), deformation potential (E_1) and carrier mobility (μ) of electrons and holes along x and y directions for pSiP/pSiAs/pSiSb.

Carrier type	m^*/m_0	C (N m^{-1})	E_1 (eV)	μ (cm^{2}V^{-1}s^{-1})
x-Electron	0.61/0.54/0.51	27.30/24.19/19.70	1.96/1.55/1.48	271.80/493.96/494.78
x-Hole	0.80/0.86/0.76	27.30/24.19/19.70	3.02/2.73/3.20	66.74/62.64/47.34
y-Electron	0.45/0.63/0.56	27.30/24.19/19.70	1.97/1.47/1.46	496.40/401.40/419.41
y-Hole	1.35/1.26/0.65	27.30/24.19/19.70	3.05/2.63/3.14	22.86/31.26/67.13

We further explored the optical properties of pSiP, pSiAs and pSiSb monolayers by computing their dielectric functions using HSE06 hybrid functional. The transverse dielectric function $\varepsilon(\omega)$ is used to describe the optical properties of materials.

$$\varepsilon(\omega) = \varepsilon_1(\omega) + i\varepsilon_2(\omega) \qquad (2),$$

where ω is the photon frequency, $\varepsilon_1(\omega)$ is the real part and $\varepsilon_2(\omega)$ is the imaginary part of dielectric function.

As shown in Figure 6, obviously, the absorption along x and y orientations are dominant. The threshold energies of dielectric function appear at around 1.91, 1.68 and 1.04 eV for pSiP, pSiAs and pSiSb monolayers, respectively. The computed threshold energies are quite close to the values of direct bandgap we computed by HSE06 functional, which also verifies the accuracy of our calculations. Furthermore, under the $\varepsilon_{xy}(\omega)$ curve of pSiP and pSiAs, high value peaks and large range absorptions near 2eV and in the 3-6 eV region, and for pSiSb, near 1eV and in the 2-5 eV region are evident. Thus, pSiP and pSiAs monolayers have high efficiency absorption of near ultraviolet and visible light; while pSiSb has efficiency absorption of visible and near infrared light. Consequently, these newly designed 2D materials are quite promising in solar cell field, photo-catalysis and other light-emitting devices.

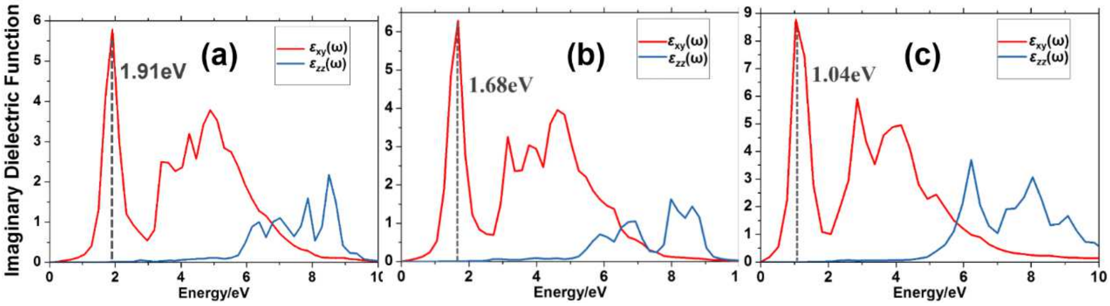

Figure 6. Imaginary parts of dielectric functions for (a) pSiP, (b) pSiAs and (c) pSiSb monolayer, respectively.

3.4. Photocatalytic activity for water-splitting

Generally, ideal photocatalysts for water-splitting should fulfill the following prerequisites,[81,82] (1) a band gap larger than 1.23 eV (potential for water-splitting reaction)[83] and smaller than 3 eV (visible light active); (2) large carrier mobility for the separation of electron-hole pair; (3) ability to harvesting the visible light; (4) band edges straddled water redox potentials,[84-89] *i.e.* the CBM energy should be higher than the reduction potential of H^+/H_2, and the VBM energy should be lower than the oxidation potential of O_2/H_2O. Moreover, the photocatalytic efficiency would be higher, if the band positions of CBM/VBM of the catalyst is closer to the reduction/oxidation potential in water splitting reaction.

Our above computations clearly demonstrated that our newly predicted pSiP and pSiAs monolayers satisfy the first three criteria: pSiP and pSiAs have direct bandgaps of 1.93 eV and 1.57 eV (HSE06), rather high carrier mobitlies, and quite efficient absorptions of visible light (since pSiSb possesses a band gap (0.95 eV) smaller than 1.23 eV), pSiSb was not considered here).

To explore the potential of pSiP and pSiAs as photocatalysts for water-splitting, we examined their band edge positions to see if they also fulfill the last criterion. Typically, the redox potentials of water-splitting reaction depends on the pH value, and they are -4.44 eV for the reduction potential (H^+/H_2), -5.67 eV for the oxidation potential (O_2/H_2O), at pH = 0.[90-91] Our computations showed that the band edges of pSiP and pSiAs (blue and red lines) are exactly straddle the water redox potentials (Figure 7, orange area). Furthermore, their CBM positions are located quite close to the reduction potential (0.05 and 0.03 eV, respectively). The difference between VBM of pSiAs and the oxidation potential is also rather small (0.3 eV), while that of pSiP and the oxidation potential is bigger (0.66 eV), which indicate that pSiP has high photocatalytic efficiency for hydrogen evolution reaction (HER), and pSiAs has both high photocatalytic efficiencies for HER and oxygen reduction reaction (ORR). In short, the computed band gaps, carrier mobility, optical absorptions and band edge positions suggest that pSiP and pSiAs are promising candidates as photocatalysts for water-splitting reaction in the visible light region.

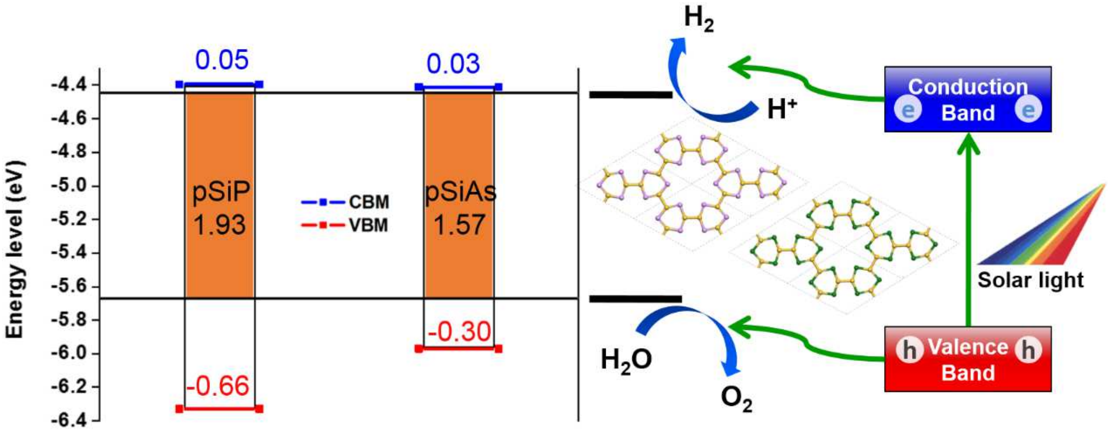

Figure 7. Band edge positions of pSiP and pSiAs monolayers. The energy scale uses the vacuum level in electron volts as reference. The CBM (blue color), VBM (red color) of materials and the redox potentials (black color) of water are presented along with the potentials in electron volts.

4. Conclusion

In summary, we have systematically investigated the stability, and electronic, optical and mechanical properties of porous silaphosphorene, silaarsenene and silaantimonene (pSiP, pSiAs and pSiSb) by means of DFT computations. The porous and planar pSiP/pSiAs/pSiSb monolayer possess aromatic Si_3P_3/Si_3As_3/Si_3Sb_3 six - membered ring, which results in their enhanced stabilities. Different from metallic silicene, pSiP, pSiAs and pSiSb have direct bandgaps of 1.93, 1.57, 0.95 eV (HSE06), respectively. Their electron carrier mobility are higher than MoS_2, which endow them great promise as electronic and optoelectronic devices. pSiP, pSiAs and pSiSb all have high efficiency absorption in visible light region, in addition, band edges of pSiP and pSiAs straddle the water redox potentials. Thus, pSiP and pSiAs monolayers are promising water-splitting photocatalysts. In short, our studies demonstrated that pSiP, pSiAs and pSiSb monolayers have excellent stabilities, unique electronic, optical and mechanical properties, which are favorable for applications in nanoelectronics, solar cells, photocatalysis for water-splitting and other optoelectronics fields.

Acknowledgement

This work was financially supported by in USA by NSF-CREST Center for Innovation, Research and Education in Environmental Nanotechnology (CIRE2N) (Grant Number HRD-1736093) and NASA (Grant 17-EPSCoRProp-0032), and in China by Innovation Project in Jiangsu Province (KYZZ16_0454).

Electronic Supplementary Information

Iso-surface of deformation electronic density of pSiP, pSiAs and pSiSb monolayers; Phonon dispersions of pSiP, pSiAs and pSiSb monolayers; The optimized geometric structure of the silicene-like SiAs and SiSb monolayers; Phonon dispersions of silicene-like SiAs and SiSb monolayers; The band structures of silicene-like SiAs and SiSb monolayers; The band structures of pSiP, pSiAs and pSiSb monolayers at PBE and HSE06 level of theory; The band structure of pSiSb monolayer including SOC effects at PBE level; Calculated values of NICS(0) and NICS(1) of $H_3Si_3P_3$, $H_3Si_3As_3$ and $H_3Si_3Sb_3$ molecules; This material is available free of charge via the internet at http://pubs.rsc.org.

Notes and References

1. K. S. Novoselov, A. K. Geim, S. V. Morozov, D. Jiang, Y. Zhang, S. V. Dubonos, I. V. Grigorieva and A. A. Firsov, *Science*, 2004, **306**, 666-669.
2. K. S. Novoselov, A. Mishchenko, A. Carvalho and A. H. Castro Neto, *Science*, 2016, **353**, aac9439.
3. S. Balendhran, S. Walia, H. Nili, S. Sriram and M. Bhaskaran, *Small*, 2015, **11**, 640-652.
4. M. Xu, T. Liang, M. Shi and H. Chen, *Chem. Rev.*, 2013, **113**, 3766-3798.
5. G. Wang, R. Pandey and S. P. Karna. *ACS Appl. Mater. Inter.*, 2015, **7**, 11490-11496.
6. L. Kou, C. Chen and S. C. Smith, *J. Phys. Chem. Lett.*, 2015, **6**, 2794-2805.
7. S. Z. Butler, S. M. Hollen, L. Cao, Y. Cui, J. A. Gupta, H. R. Gutierrez, T. F. Heinz, S. S. Hong, J. Huang, A. F. Ismach, E. Johnston-Halperin, M. Kuno, V. V. Plashnitsa, R. D. Robinson, R. S. Ruoff, S. Salahuddin, J. Shan, L. Shi, M. G. Spencer, M. Terrones, W. Windl and J. E. Goldberger, *ACS Nano*, 2013, **7**, 2898-2926.
8. A. Carvalho, M. Wang, X. Zhu, A. S. Rodin, H. B. Su and A. H. C. Neto, *Nat. Rev. Mater.*, 2016, **1**, 16061.
9. Y. Jing, X. Zhang and Z. Zhou, *Wires. Comput. Mol. S.*, 2016, **6**, 5-19.
10. A. Molle, J. Goldberger, M. Houssa, Y. Xu, S. C. Zhang and D. Akinwande, *Nat. Mater.*, 2017, **16**, 163-169.
11. Y. Yang, S. Umrao, S. Lai and S. Lee, *J. Phys. Chem. Lett.*, 2017, **8**, 859-865.

12. A. J. Mannix, B. Kiraly, M. C. Hersam and N. P. Guisinger, *Nat. Rev. Chem.*, 2017, **1**, 0014.

13. Q. Tang, Z. Zhou and Z. F. Chen, *Wires. Comput. Mol. Sci.*, 2015, **5**, 360-379.

14. M. Pumera and Z. Sofer, *Adv. Mater.*, 2017, **29**, 1605299

15. C. Tan, X. Cao, X.-J. Wu, Q. He, J. Yang, X. Zhang, J. Chen, W. Zhao, S. Han and G.-H. Nam, *Chem. Rev.*, 2017, **117**, 6225-6331.

16. G. G. Guzmán-Verri and L. C. Lew Yan Voon, *Phys. Rev. B*, 2007, **76**, 075131.

17. J. J. Zhao, H. S. Liu, Z. M. Yu, R. G. Quhe, S. Zhou, Y. Y. Wang, C. C. Liu, H. X. Zhong, N. N. Han, J. Lu, Y. G. Yao and K. H. Wu, *Prog. Mater. Sci.*, 2016, **83**, 24-151.

18. L. Chen, C. C. Liu, B. Feng, X. He, P. Cheng, Z. Ding, S. Meng, Y. Yao and K. Wu, *Phys. Rev. Lett.*, 2012, **109**, 056804.

19. P. De Padova, P. Vogt, A. Resta, J. Avila, I. Razado-Colambo, C. Quaresima, C. Ottaviani, B. Olivieri, T. Bruhn and T. Hirahara, *Appl. Phys. Lett.*, 2013, **102**, 163106.

20. E. Durgun, S. Tongay and S. Ciraci, *Phys. Rev. B*, 2005, **72**, 075420.

21. S. Cahangirov, M. Topsakal, E. Akturk, H. Sahin and S. Ciraci, *Phys. Rev. Lett.*, 2009, **102**, 236804.

22. K. Takeda and K. Shiraishi, *Physical review. B, Condens. Matter Mater. Phys.*, 1994, **50**, 14916-14922.

23. U. Rothlisberger, W. Andreoni and M. Parrinello, *Phys. Rev. Lett.*, 1994, **72**, 665-668.

24. B. Aufray, A. Kara, S. Vizzini, H. Oughaddou, C. Léandri, B. Ealet and G. Le Lay, *Appl. Phys. Lett.*, 2010, **96**, 183102.

25. C. Leandri, G. Le Lay, B. Aufray, C. Girardeaux, J. Avila, M. Davila, M. Asensio, C. Ottaviani and A. Cricenti, *Surf. Sci.*, 2005, **574**, L9-L15.

26. G. Le Lay, B. Aufray, C. Léandri, H. Oughaddou, J.-P. Biberian, P. De Padova, M. Dávila, B. Ealet and A. Kara, *Appl. Surf. Sci.*, 2009, **256**, 524-529.

27. B. Lalmi, H. Oughaddou, H. Enriquez, A. Kara, S. Vizzini, B. Ealet and B. Aufray, *Appl. Phys. Lett.*, 2010, **97**, 223109.

28. C.-L. Lin, R. Arafune, K. Kawahara, N. Tsukahara, E. Minamitani, Y. Kim, N. Takagi and M. Kawai, *Appl. Phys. Express*, 2012, **5**, 045802.

29. B. Feng, Z. Ding, S. Meng, Y. Yao, X. He, P. Cheng, L. Chen and K. Wu, *Nano Lett.*, 2012, **12**, 3507-3511.

30. G. Le Lay, *Nat. nanotechnol.*, 2015, **10**, 202-203.

31. L. Tao, E. Cinquanta, D. Chiappe, C. Grazianetti, M. Fanciulli, M. Dubey, A. Molle and D. Akinwande, *Nat. nanotechnol.*, 2015, **10**, 227-231.

32. H. Liu, A. T. Neal, Z. Zhu, Z. Luo, X. Xu, D. Tománek and P. D. Ye, *ACS Nano*, 2014, **8**, 4033-4041.

33. L. Li, Y. Yu, G. J. Ye, Q. Ge, X. Ou, H. Wu, D. Feng, X. H. Chen and Y. Zhang, *Nat. nanotechnol.*, 2014, **9**, 372-377.

34. R. Fei and L. Yang, *Nano Lett.*, 2014, **14**, 2884-2889.

35. Z.-Y. Ong, Y. Cai, G. Zhang and Y.-W. Zhang, *J. Phys. Chem. C*, 2014, **118**, 25272-25277.

36. L. Wang, A. Kutana, X. Zou and B. I. Yakobson, *Nanoscale*, 2015, **7**, 9746-9751.

37. L. Kou, Y. Ma, S. C. Smith and C. Chen, *J. Phys. Chem. Lett.*, 2015, **6**, 1509-1513.

38. D. Warschauer, *J. Appl. Phys.*, 1963, **34**, 1853-1860.

39. S. Narita, Y. Akahama, Y. Tsukiyama, K. Muro, S. Mori, S. Endo, M. Taniguchi, M. Seki, S. Suga and A. Mikuni, *Physica B+ C*, 1983, **117**, 422-424.

40. Y. Maruyama, S. Suzuki, K. Kobayashi and S. Tanuma, *Physica B+ C*, 1981, **105**, 99-102.

41. S. Zhang, S. Guo, Z. Chen, Y. Wang, H. Gao, J. Gómez-Herrero, P. Ares, F. Zamora, Z. Zhu, H. Zeng, *Chem. Soc. Rev.* **2018**, ASAP, DOI: 10.1039/C7CS00125H

42. S. Zhang, Z. Yan, Y. Li, Z. Chen and H. Zeng, *Angew. Chem.*, 2015, **54**, 3112-3115.

43. S. Zhang, M. Xie, F. Li, Z. Yan, Y. Li, E. Kan, W. Liu, Z. Chen and H. Zeng, *Angew. Chem.*, 2016, **55**, 1666-1669.

44. H. S. Tsai, C. W. Chen, C. H. Hsiao, H. Ouyang and J. H. Liang, *Chem Commun.*, 2016, **52**, 8409-8412.

45. P. Ares, F. Aguilar-Galindo, D. Rodriguez-San-Miguel, D. A. Aldave, S. Diaz-Tendero, M. Alcami, F. Martin, J. Gomez-Herrero and F. Zamora, *Adv. Mater.*, 2016, **28**, 6332-6336.

46. C. Gibaja, D. Rodriguez-San-Miguel, P. Ares, J. Gomez-Herrero, M. Varela, R. Gillen, J. Maultzsch, F. Hauke, A. Hirsch, G. Abellan and F. Zamora, *Angew. Chem.*, 2016, **55**, 14345-14349.

47. J. Ji, X. Song, J. Liu, Z. Yan, C. Huo, S. Zhang, M. Su, L. Liao, W. Wang, Z. Ni, Y. Hao and H. Zeng, *Nat. Commun.*, 2016, **7**, 13352.

48. M. Grätzel, *Nature*, 2001, **414**, 338-344.

49. A. J. Nozik, J. Miller, *Chem. Rev.* 2010, **110**, 6443-6445.

50. M. G. Walter, E. L. Warren, J. R. McKone, S. W. Boettcher, Q. Mi, E. A. Santori and N. S. Lewis, *Chem. Rev.*, 2010, **110**, 6446-6473.

51. X. Chen, S. Shen, L. Guo and S. S. Mao, *Chem. Rev.*, 2010, **110**, 6503-6570.

52. B. Sa, Y.-L. Li, J. Qi, R. Ahuja and Z. Sun, *J. Phys. Chem. C*, 2014, **118**, 26560-26568.

53. M. Z. Rahman, C. W. Kwong, K. Davey and S. Z. Qiao, *Energy Environ. Sci.*, 2016, **9**, 709-728.

54. A. E. Seitz, M. Eckhardt, A. Erlebach, E. V. Peresypkina, M. Sierka and M. Scheer, *J. Am. Chem. Soc.*, 2016, **138**, 10433-10436.

55. G. Kresse and J. Hafner, *Phys. Rev. B*, 1993, **47**, 558-561.

56. P. E. Blochl, *Phys. Rev. B*, 1994, **50**, 17953-17979.

57. J. P. Perdew, K. Burke and M. Ernzerhof, *Phys. Rev. Lett.*, 1996, **77**, 3865.

58. M. D. Segall, P. J. D. Lindan, M. J. Probert, C. J. Pickard, P. J. Hasnip, S. J.Clark and M. C. Payne, *J. Phys.: Condens. Matter.*, 2002, **14**, 2717-2744.

59. B. Delley, *J. Chem. Phys.*, 1990, **92**, 508-517.

60. B. Delley, *J. Chem. Phys.*, 2000, **113**, 7756-7764.

61. Y. Wang, J. Lv, L. Zhu and Y. Ma, *Phys. Rev. B*, 2010, **82**, 094116.

62. C. Filippi, D. J. Singh and C. J. Umrigar, *Phys. rev. B*, 1994, **50**, 14947-14951.

63. J. Heyd, G. E. Scuseria and M. Ernzerhof, *J. Chem. Phys.*, 2003, **118**, 8207-8215.

64. Y. Guo, S. Zhang and Q. Wang, *Phys. Chem. Chem. Phys.*, 2014, **16**, 16832-16836.

65. Y. Ding and Y. Wang, *J. Phys. Chem. C*, 2013, **117**, 18266-18278.

66. A. Savin, R. Nesper, S. Wengert and T. F. Fassler, *Angew. Chem.*, 1997, **36**, 1809-1832.

67. N. Drummond, V. Zolyomi and V. Fal'Ko, *Phys. Rev. B*, 2012, **85**, 075423.

68. Y. Wang, F. Li, Y. Li and Z. Chen, *Nat. Commun.*, 2016, **7**, 11488.

69. C. Kamal and M. Ezawa, *Phys. Rev. B*, 2015, **91**, 085423.

70. O. Ü. Aktürk, V. O. Özçelik and S. Ciraci, *Phys. Rev. B*, 2015, **91**, 235446.

71. S. Zhang, S. Guo, Y. Huang, Z. Zhu, B. Cai, M. Xie, W. Zhou and H. Zeng, *2D Materials*, 2016, **4**, 015030.

72. B. Huang, H. L. Zhuang, M. Yoon, B. G. Sumpter and S.-H. Wei, *Phys. Rev. B*, 2015, **91**, 121401.

73. F. Schwierz, *Nat. Nanotechnol.*, 2010, **5**, 487-496.

74. J. Chen, J. Xi, D. Wang, Z. Shuai, *J. Phys. Chem. Lett.*, 2013, **4**, 1443-1448.

75. Y. Cai, G. Zhang and Y.-W. Zhang, *J. Am. Chem. Soc.* 2014, **136**, 6269-6275.

76. B. Radisavljevic, A. Radenovic, J. Brivio, i. V. Giacometti and A. Kis, *Nat.*

Nanotechnol., 2011, **6**, 147-150.

77. J. Bardeen and W. Shockley, *Phys. Rev.*, 1950, **80**, 72.
78. M.-Q. Long, L. Tang, D. Wang, L. Wang and Z. Shuai, *J. Am. Chem. Soc.*, 2009, **131**, 17728-17729.
79. M. Long, L. Tang, D. Wang, Y. Li and Z. Shuai, *ACS nano*, 2011, **5**, 2593-2600.
80. J. Qiao, X. Kong, Z.-X. Hu, F. Yang and W. Ji, *Nat. commun.*, 2014, **5**.
81. J. Wang, J. Meng, Q. Li and J. Yang, *Phys. Chem. Chem. Phys.*, 2016, **18**, 17029-17036.
82. X. Li, Z. Li and J. Yang, *Phys. rev. Lett.*, 2014, **112**, 018301.
83. X. Wang, K. Maeda, A. Thomas, K. Takanabe, G. Xin, J. M. Carlsson, K. Domen and M. Antonietti, *Nat. Mater.*, 2009, **8**, 76-80.
84. A. K. Singh, K. Mathew, H. L. Zhuang and R. G. Hennig, *J. Phys. Chem. Lett.*, 2015, **6**, 1087-1098.
85. B. Luo, G. Liu and L. Wang, *Nanoscale*, 2016, **8**, 6904-6920.
86. X. Zhang, X. Zhao, D. Wu, Y. Jing and Z. Zhou, *Adv. Sci.*, 2016, **3**, 1600062.
87. M. Ni, M. K. Leung, D. Y. Leung and K. Sumathy, *Renew. Sust. Energ. Rev.*, 2007, **11**, 401-425.
88. X. Li, J. Zhao and J. Yang, *Sci.Rep.*, 2013, **3**, 1858.
89. J. Wang, Z. Guan, J. Huang, Q. Li and J. Yang, *J. Mater. Chem. A*, 2014, **2**, 7960-7966.
90. H. L. Zhuang and R. G. Hennig, *Chem. Mater.*, 2013, **25**, 3232-3238.

91. V. Chakrapani, J. C. Angus, A. B. Anderson, S. D. Wolter, B. R. Stoner and G. U. Sumanasekera, *Science*, 2007, **318**, 1424-1430.